Coverage in mmWave Cellular Networks With Base Station Co-Operation

Diana Maamari, Natasha Devroye, and Daniela Tuninetti

***Abstract*—Signal outage, due to shadowing and blockage, is expected to be the main bottleneck in millimeter wave (mmWave) networks. Moreover, the anticipated dense deployment of base stations in mmWave networks is expected to increase the interference from strong line-of-sight base stations too, thus further increasing the probability of outage. To address the issue of reducing outage, this paper explores the possibility of base station co-operation in the downlink of mmWave heterogenous networks. The main focus of this work is showing that, in a stochastic geometry framework that incorporates blockage, co-operation from randomly located base stations decreases the probability of outage/increases the coverage probability. Coverage probabilities are derived accounting for: blockage, different fading distributions on the direct links (but always Rayleigh fading on the interference links), antenna directionality, and different tiers. Numerical results suggest that coverage with base station co-operation in dense mmWave systems (i.e., with high average number of base stations per square meter), without small scale fading on the direct communications links, and with any probability of signal blockage, considerably exceeds coverage without co-operation. In contrast, a small increase in coverage is reported when mmWave networks are less dense, have a high probability of signal blockage and the direct communications links are affected by Rayleigh fading.**

***Index Terms*—Coordinated multipoint, coverage probability, joint transmission, millimeter wave, uniform linear arrays, 5G.**

I. Introduction

ONE of the fundamental goals for 5G is a radical increase in data rates [1]. It is anticipated that higher data rates will be achieved by extreme densification of base stations, massive multiple-input-multiple-output (MIMO), increased data rate and/or base station cooperation [1]. However, prime microwave wireless spectrum has become severely limited, with little unassigned bandwidth available for emerging wireless products and services. Therefore, to fulfill the need for increased bandwidth, millimeter wave (mmWave) spectrum between 30 and 300 GHz are being considered for future 5G wireless mobile networks. Until recently, mmWave frequency bands were presumed to be unreliable for cellular communication due to blockage, absorption, diffraction, and penetration, resulting in outages and unreliable cellular coverage [2]. However, advances in CMOS radio-frequency circuits, along with the very small wavelength of mmWave signals, allows for the packing of large antenna arrays at both the transmit and receive ends, thus providing highly directional beam forming gains and acceptable signal-to-noise ratio (SNR) [2], [3]. This directionality is expected to reduce interference when compared to microwave networks [2]. It is thus anticipated that mmWave spectrum holds tremendous potential for providing multi-Gigabits-per-second data rates in upcoming cellular systems [4].

MmWave networks are envisioned to be dense and heterogeneous, with a variety of different types of users including low power nodes, relays and device-to-device (D2D), etc., all being incorporated into the 5G mmWave networks [5]. Each different type of users may require different quality of service (QoS) levels, and may have different types of backhauls [6]. It is thus reasonable to model these networks as having different tiers of base stations.

Cooperation between macro, pico and femto base stations has been proposed to enable a uniform broadband user experience across the network, and coordination among different tiers will be a key requirement to mitigate interference in dense 5G networks [5]. With cooperation, receivers will be allowed to have a dual connectivity by simultaneously connecting to the base station from a macrocell and that from small cell for either uplink and downlink communications [5]. In this work we thus consider different tiers of cooperating base stations.

Since cooperation in mmWave network has been proposed for 5G networks [5] and since existing results for cooperation in microwave networks can not be leveraged to infer its impact on mmWave networks (due to, for example, the fact that the mmWave networks have sparse channel matrices and are highly affected by blockage [7]), in this work we account for the distinctive features of mmWave networks compared to microwave networks and characterize the coverage probability. Our analysis aims to unveil when cooperation is beneficial and when it provides minimal gain.

A. Past Work

MmWave cellular systems and CoMP networks have been studied in the past. In [4] the authors compared the performance, in terms of coverage and capacity, of a stochastic geometry based mmWave network without CoMP to a microwave

Manuscript received March 20, 2015; revised August 19, 2015, November 2, 2015, and December 28, 2015; accepted December 30, 2015. Date of publication January 4, 2016; date of current version April 7, 2016. This work was supported by NSF under Grant 1017436, Grant 1216825, and Grant 1422511. The associate editor coordinating the review of this paper and approving it for publication was L. Lai.

D. Maamari was with the Department of Electrical and Computer Engineering, University of Illinois at Chicago (UIC), Chicago, IL 60607 USA. She is now with Huawei Technologies, Rolling Meadows, IL USA (e-mail: Diana.Maamari@huawei.com).

N. Devroye and D. Tuninetti are with Department of Electrical and Computer Engineering, University of Illinois at Chicago (UIC), Chicago, IL 60607 USA (e-mail: devroye@uic.edu; danielat@uic.edu).

Color versions of one or more of the figures in this paper are available online at http://ieeexplore.ieee.org.

Digital Object Identifier 10.1109/TWC.2016.2514347

cellular network, at a single antenna typical user/receiver. In [4], directionality at the transmitters, intra-cell and inter-cell interference were accounted for but blockage was not included in the analysis; it was show that coverage in mmWave systems increases with the decrease in the half-power beam width of the radiation pattern. In fact, having narrower beams decreases beam overlap, thus decreasing intra-cell and inter-cell interference and increasing coverage probability. In this paper, we propose to study the problem of base station cooperation in the downlink of dense mmWave heterogenous network as a means to combat blockage and decrease signal outage. Our derivations of the coverage probability, similarly to [4], account for interference experienced at the typical user, but in addition blockage is incorporated in the analysis.

In [7], [8] the authors proposed a stochastic geometry framework to evaluate the performance of mmWave cellular networks with blockage but without CoMP. The authors incorporated blockage by modeling the probability of a communication link – being either a line-of-sight (LOS) or non-LOS (NLOS) link – as function of the length of the communication link from the serving base station. Different pathloss laws were applied to the LOS and NLOS links. Numerical results in [8] suggested that higher data rates can be achieved when compared to microwave cellular networks. One of the interesting observations made is that mmWave networks should be dense but not too dense since the number of LOS interfering base stations increases when the density of base stations increases. In this paper, we follow the modeling approach of [8] to incorporate blockage and to differentiate between LOS links and NLOS links from the base stations in the analysis of joint transmission in mmWave networks.

In [9], [10] the authors used stochastic geometry to study microwave (but not mmWave) with joint transmission CoMP where single antenna base stations transmit the same data to single antenna users. Different performance metrics were considered to evaluate the performance at the typical user located at an arbitrary location (referred to as the general user) and receiving data from base stations with the strongest average received power. A user at the cell-corner (referred to as a worst-case user) was also considered. The coverage probability was derived for both types of users under the assumption that the base stations have no CSI. The case with full CSI was evaluated with different performance metrics (diversity gain and power gain). In this paper, the derivation of the coverage probability for a mmWave network with base station cooperation parallels that in [9] for the general user, except that key factors specific to the mmWave channel have to incorporated, namely blockage, highly directional transmission at the base stations, and different fading distributions for the direct links to model various amount of scattering.

The authors in [3] considered the problem of finding suitable single-user MIMO transmit precoding and receive combining matrices in mmWave systems under a set of hardware constraints suitable for large antenna arrays. The proposed design consists of: the transmitter applies a number of array response vectors at the RF level (which are phase only vectors) and forms linear combinations of these vectors using a digital precoder. A similar approach was developed in [11] for a multiuser MIMO downlink. In this paper, the cooperating base stations are modeled to beam steer (precode with phase only vectors) to the typical user and the receivers to apply a single combining vector (not necessarily a phase only vector) to process the received signal from the cooperating base stations.

B. Main Contributions

We study the benefits of base station cooperation in the downlink of a heterogenous mmWave cellular system as a means to decrease signal outage. To do so we incorporate the key factors specific to a mmWave system into the stochastic geometry based model of [4], [7]–[10], [12], namely: blockage by incorporating LOS and NLOS base stations, uniform linear arrays for highly directional transmission, and different fading distributions for the direct links while keeping Rayleigh fading on the interfering links. We consider single path channel models, which could be either LOS or NLOS. We formulate the problem for general MIMO receivers as well, but for sake of analytical tractability only the single antenna case in studied in this work. Integral expressions for the coverage probabilities are derived for the typical user with different fading distributions for the direct links (namely, Rayleigh, Nakagami and no fading) in the presence of blockage.

CoMP is expected to provide a substantial gain in coverage with the anticipated improved fading distribution and extreme base station densification in the presence of blockage. Our extensive numerical examples show that this is in fact the case for the following scenarios: (A) for dense mmWave networks where the number of interfering LOS base stations increases, and (B) when there is no small scale fading channel on the channel gains from the cooperating base stations (a good assumption due to the high directional transmission). We also provide examples when cooperation does not provide substantial increase in coverage probability.

We also observe that: (1) for noise limited networks base station cooperation does not provide substantial increase in coverage probability. This may be understood as follows: the gain from cooperation comes from the fact that it transforms the strongest interferers into cooperative links; since there is no interference in a noise limited system, the gain is subsequently negligible. Moreover, the fact that cooperating base stations are farther apart and experience higher path loss decreases the received power further, decreasing the cooperation gain. Also, (2) in the absence of blockage, the amount of increase in coverage probability with base station cooperation decreases with an increase in the number of transmit antennas. This may be understood as follows: with highly directional transmission interference is limited and therefore the gain from cooperation is limited as well.

C. Paper Organization

The downlink CoMP mmWave heterogenous network model, the beam steering at the base stations and the decoding at the typical user are explained in Section II. The coverage probability where each tier experiences blockage, and with the Rayleigh

TABLE I
POISSON POINT PROCESS VARIABLES

Notation	Description
K	Total number of tiers
Φ_k	Homogenous Poisson Point Process (PPP) indexed by $k \in [1:K]$
λ_k	Intensity of the PPP Φ_k $k \in [1:K]$
P_k	Available power at each base station that belongs to tier $k \in [1:K]$
v	Points in 2D plane representing location of base stations
$\|v\|$	Distance from point v to the typical user located at the origin
α	Pathloss exponent random variable
α_{LOS}, α_{NLOS}	Pathloss exponent for LOS and NLOS links, respectively
β_k	Blockage parameter for tier $k \in [1:K]$
$f(v)$	Function that returns the tier index to which a base station at v belongs to
$\gamma_v = \frac{P_{f(v)}}{\|v\|^{\alpha}}$	Received power at typical user from base station at location v
$\Theta_k = \{\frac{1}{\gamma_v}, v \in \Phi_k\}$	Set of inverse of pathloss between each base station in Φ_k $k \in [1:K]$ and the typical user
$\Theta = \cup_{k=1}^{K} \Theta_k$	Non-homogenous PPP representing the union of homogenous PPP's
$f_{\Gamma}(\cdot)$	Joint distribution of $\Gamma = \{1/\gamma_{v_i}, i \in [1:N]\}$ for the n cooperating base stations

TABLE II
GENERAL CHANNEL MODEL VARIABLES

Notation	Description
N_t, N_r	Number of antennas at each base station and at the typical receiver
$\mathbf{H}_v$	MIMO channel from base station at location v to typical user
h_v	Small scale fading from base station at location v to typical user
L_v	Number of channel clusters from base station at location v to typical user
ϕ_v^t	Path angle at the transmitter of base station at location v to typical user
ϕ_v^r	Path angle at the typical user from base station at location v
$\Omega_{\phi} = \cos(\phi)$	Directional cosine
$\mathbf{a}_{t(r)}(.)$	Uniform linear array vector at the transmitter (receiver)
$\Delta_{t(r)}$	Normalized transmit (receive) antenna separation
$A_{t(r)}$	Normalized length of the transmit (receive) antenna array
$\mathbf{n}$	Noise vector of i.i.d $\mathcal{CN}(0, \sigma_n^2)$

TABLE III
CHANNEL VARIABLES FROM CO-OPERATING BASE STATIONS

Notation	Description
$\mathcal{T}$	Set of cooperating base stations with cardinality $\|\mathcal{T}\| = n$
v_i	Location of cooperating base station $i \in \mathcal{T}$
$\mathbf{H}_{v_i}$	MIMO channel from cooperating base station $i \in \mathcal{T}$
$\mathbf{X}_{v_i}$	Transmit signal from cooperating base stations $i \in \mathcal{T}$
$h_{v_i}, \phi_{v_i}^t, \phi_{v_i}^r, \gamma_{v_i}$	Channel parameters for cooperating base stations $i \in \mathcal{T}$ as defined in Table II

fading assumption (outdoor rich scattering scenario) is derived in Section III. In Section IV, we derive the coverage probability for the same network model but use the Nakagami fading distribution to model the fading distribution on the direct links of the cooperating base stations (outdoor limited scattering scenario). The assumption of having no small scale fading (indoor scenario) for the channel gains from the cooperating base stations is further considered in Section V. Proofs may be found in the Appendices.

II. SYSTEM MODEL

Tables I, II, III, and IV summarize the notation used throughout the paper.

A. Network Model

Consider a K-tier heterogenous network where each tier is an independent two-dimensional homogenous Poisson point process (PPP). We denote the base station location process of tier k, $k \in [1:K]$, by Φ_k. The mmWave base stations that belong to the same tier k transmit with the same power P_k for $k \in [1:K]$, i.e., base stations belonging to different tiers have different transmission power so as to model the network heterogeneity. The multi-tiers are overlaid and have different average cell radii r_k, which result in different intensities $\lambda_k = \frac{1}{\pi r_k^2}$ for $k \in [1:K]$ [9]. In the following intensity and density are used interchangeably.[1]

Each tier is characterized by a non-negative blockage constant β_k for $k \in [1:K]$. The parameter β_k is determined by the density and average size of objects within the tier and where the average LOS range is given by $1/\beta_k$ [7], [8], [13]. The probability of the communication link being a LOS link (no blockage on the link) within tier k is $\mathbb{P}(\text{LOS}_k) = e^{-\beta_k r}$, where r represents the length of the communication link, while the probability of a link being NLOS is $\mathbb{P}(\text{NLOS}_k) = 1 - \mathbb{P}(\text{LOS}_k)$. The LOS and

[1]The number λ_k represents the average number of base stations per meter square in tier k and is inversely proportional to the average cell radius of a tier k cell. If $\lambda_1 > \lambda_2$, then tier 1 is said to be *denser* than tier 2. In other words, tier 1 has on average a higher number of base stations per meter square than tier 2. Therefore, the number of interfering base stations on average in tier 1 is greater than that in tier 2.

TABLE IV
CHANNEL VARIABLES FROM INTERFERING BASE STATIONS

Notation	Description
l_i	Location of interfering base station $i \notin \mathcal{T}$
$\mathbf{H}_{l_i}$	MIMO channel from interfering base station $i \notin \mathcal{T}$
$\mathbf{X}_{l_i}$	Transmit signal from interfering base station $i \notin \mathcal{T}$
$h_{l_i}, \phi^t_{l_i}, \phi^r_{l_i}, \gamma_{l_i}$	Channel parameters from interfering base station $i \notin \mathcal{T}$ as defined in Table II
$\theta^t_{l_i}$	Angle used by interfering base station $i \notin \mathcal{T}$ to beam steer to a user other than typical user

NLOS links will have different pathloss exponents, α_{LOS} and α_{NLOS}, respectively, and are the same for all $k \in [1 : K]$.

We study the coverage probability as experienced by the typical user located at the origin, and denote the set of cooperating base stations, which jointly transmit to the typical user, by $\mathcal{T} \subset \cup_{k=1}^{K} \Phi_k$. We assume that $|\mathcal{T}| = n$, and that these n base-stations correspond to those with the strongest received power at the typical user receiver (thus not neccesarily belonging to n different tiers). In the rest of the section, we first describe the channel model and then derive the output signal at the typical user's receiver.

B. Single Path Channel Model

The clustered channel model has been used to model the mmwave wireless channel between the base stations and the typical user [3], [7], [14]. In this analysis, however, we consider the single path channel model. This path could be either LOS or NLOS. The more general case with multiple clusters might result in different conclusions. We assume that all base stations have the same number of transmit antennas N_t, while the receiver has N_r receive antennas. The $N_r \times N_t$ channel matrix $\mathbf{H}_v$, between a base station located at $v \in \mathbb{R}^2$ and the typical user, we consider in this analysis, is the single path channel which is expressed as

$$\mathbf{H}_v = \sqrt{N_t N_r}\sqrt{\gamma_v} h_v \mathbf{a}_r(\phi^r_v)\, \mathbf{a}_t(\phi^t_v)^*. \tag{1}$$

In the following for simplicity we use the following notation:

- $\gamma_v = \frac{P_{f(v)}}{\|v\|^\alpha}$ is the receive signal power for the signal sent by the base station at location v,
- $\|v\|$ is the distance from the base station at location v to the user at the origin,
- similarly, $\|v_i\|$ is the distance from the base station at location v_i to the user at the origin,
- $f(v)$ is a function that returns the tier index k of the tier to which the base station at location v belongs,
- α is the pathloss exponent. The pathloss α is a random variable that takes on values α_{LOS} and α_{NLOS} with probability $e^{-\beta_k v}$ and $1 - e^{-\beta_k v}$, respectively,
- h_v is the complex small scale fading channel gain,
- the vectors $\mathbf{a}_i(\phi^i_v)$, $i \in \{r, t\}$, are the normalized uniform linear array (ULA) transmit and receive array response and are given by [15, Eq. (7.21), Eq. (7.25)]

$$\mathbf{a}_i(\phi^i_v) = \frac{1}{\sqrt{N_i}}\left[1, e^{-jA_i}, \ldots, e^{-j(N_i-1)A_i}\right]^T, \tag{2}$$

where $A_i = 2\pi\Delta_i \cos(\phi^i_v)$ is the normalized length of the array, and Δ_i is the normalized antenna separation (normalized to the unit of the carrier wavelength) at a path angle ϕ^i_v.

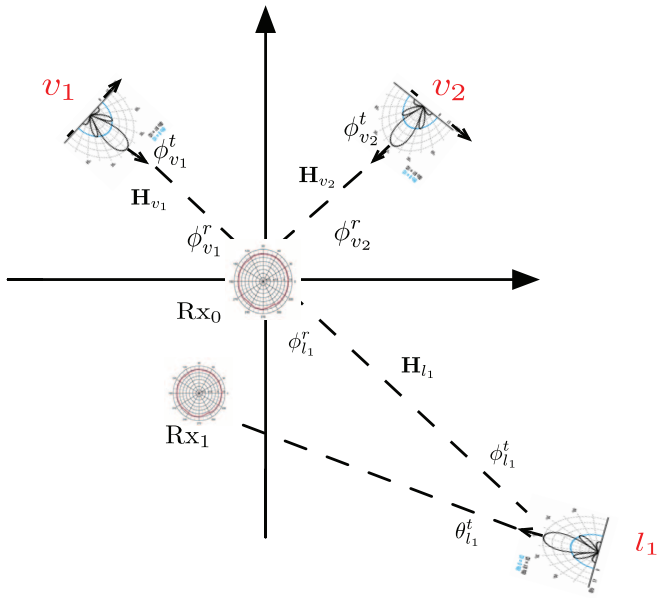

Fig. 1. A typical user is served by two cooperating base stations at locations v_1 and v_2, while being interfered by base station at location l_1.

C. Received Signal at the Typical User

In this section we further divide the points $v \in \mathbb{R}^2$ into a set of points v_i and l_i to differentiate between the location of the cooperating and interfering base stations, respectively. The $N_r \times N_t$ desired channel matrices are denoted by $\mathbf{H}_{v_i}$ for $i \in \mathcal{T}$, where $n = |\mathcal{T}|$ is a positive constant, while the interfering channel matrices are denoted by $\mathbf{H}_{l_i}$ for $i \notin \mathcal{T}$. To clarify the notation, Fig. 1 shows an example of a network model, where two base stations at locations v_1 and v_2, jointly transmit to the typical receiver located at the origin (indicated as Rx_0) in the presence of a single interfering base station at location l_1. The MIMO channel matrices between the cooperating base stations and the typical user are given by $\mathbf{H}_{v_1}$ and $\mathbf{H}_{v_2}$. The channel matrix between the interfering base station and the typical user is denoted by $\mathbf{H}_{l_1}$. The angles, $\phi^t_{v_i}$ and $\phi^r_{v_i}$, are the cluster's angle of departure and arrival respectively from the base station v_i, $i \in [1 : 2]$, to the typical receiver. The angle $\phi^t_{l_1}$ is the angle of departure of the cluster from the interfering base station. The base station at l_1 uses a beam steering angle θ_{l_1} to transmit data to some other user (not the typical user) indicated as Rx_1.

The received signal is

$$\mathbf{y} = \sum_{i\in\mathcal{T}} \sqrt{N_t N_r}\sqrt{\gamma_{v_i}} h_{v_i}\, \mathbf{a}_r(\phi^r_{v_i})\, \mathbf{a}_t(\phi^t_{v_i})^* \mathbf{X}_{v_i} + \sum_{i\notin\mathcal{T}} \sqrt{N_t N_r}\sqrt{\gamma_{l_i}} h_{l_i}\, \mathbf{a}_r(\phi^r_{l_i})\, \mathbf{a}_t(\phi^t_{l_i})^* \mathbf{X}_{l_i} + \mathbf{n}, \tag{3}$$

where the first sum in (3) is the desired signal from the cooperating base stations, while the second sum contains the signals from the interfering base stations, and $\mathbf{n}$ is the noise vector of i.i.d $\mathcal{CN}(0, \sigma^2)$ components.

The user associates with a set of cooperating base stations $\mathcal{T}$ that provide the strongest average received power [10]

$$\mathcal{T} = \arg \max_{\{v_1 \cdots v_n\} \subset \cup_{k=1}^{K} \Phi_k} \sum_{i=1}^{n} \frac{P_{f(v_i)}}{\|v_i\|^{\alpha}}, \tag{4}$$

and $\mathcal{T}^c := \cup_{k=1}^{K} \Phi_k \setminus \mathcal{T}$. The path angles, $\phi_{v_i}^t$, $i \in \mathcal{T}$, and $\phi_{l_i}^t$, $i \notin \mathcal{T}$, represent the angle of departure of the desired and interfering paths, respectively, while $\phi_{v_i}^r$, $i \in \mathcal{T}$, and $\phi_{l_i}^r$, $i \notin \mathcal{T}$, represent the angle of arrival of the received path from the cooperating and interfering base stations, respectively. The transmit signals, $\mathbf{X}_{v_i}$, $i \in \mathcal{T}$ and $\mathbf{X}_{l_i}$, $i \notin \mathcal{T}$, represent the signal from the cooperating and interfering base stations within $\mathcal{T}$ and $\mathcal{T}^c$, respectively.

D. Beam Steering

The base stations in $\mathcal{T}$ jointly send the same data to the receiver. Each base station beam steers to the typical user, therefore the transmitted signal is

$$\mathbf{X}_{v_i} = \mathbf{a}_t\left(\phi_{v_i}^t\right) s, \quad i \in \mathcal{T}, \tag{5}$$

where s is symbol transmitted by the cooperating base stations to the typical receiver. The signals transmitted by the interfering base stations are

$$\mathbf{X}_{l_i} = \mathbf{a}_t\left(\theta_{l_i}^t\right) s_{l_i}, \quad i \notin \mathcal{T}, \tag{6}$$

where s_{l_i} is the channel input symbol transmitted by the interfering base stations, while the angle $\theta_{l_i}^t$ is the angle used by base station l_i to beam steer to a user other than the typical user, and is different from $\phi_{l_i}^t$ in general. We assume that s and s_{l_i} are independent zero mean and unit variance random variables.

Assumption 1: The cooperating base stations have perfectly beam steered to the typical receiver: notice that the angles in (5), used by the base station to beam steer, are equal to the clusters' angles of departure in the desired channel in (3).

E. Decoding

The receiver uses the vector $\mathbf{w} \in \mathbb{C}^{N_r \times 1}$ to detect the scalar transmit symbol s by processing the received signal $\mathbf{y}$ as

$$\widehat{y} = \mathbf{w}^* \mathbf{y}, \quad \mathbf{w} = \sum_{j=1}^{n} \mathbf{a}_r\left(\phi_{v_j}^r\right). \tag{7}$$

Remark 1: The choice of $\mathbf{w}$ in (7) is one choice of a linear decoder that can be implemented using an RF (analog) and base band (digital) combiner. If one wants to consider a decoder with better performance, then the work in [3], which finds a hybrid MIMO receiver combining algorithm and minimizes the mean-square-error between the transmitted and received signals under a set of RF hardware constraints for the resulting point-to-point channel should be generalized to finding a suitable algorithm for the downlink cooperative channel in the presence of interference.

Assumption 2: We assume perfect CSI of the path angles at the decoders since these angles vary slowly. However, we assume that the phases of the complex channel gains, h_{v_i}, $i \notin \mathcal{T}$, are not available at the terminals as they change very quickly on the order of a wavelength and thus cannot be tracked. The performance here should be considered as an upper bound on the performance of the more realistic case with imperfect path angle knowledge.

F. Output Signal

The output signal at the typical user under the previously stated assumptions is given by

$$\begin{aligned}\hat{y} &= \mathbf{w}^* \mathbf{y} \\ &= \sqrt{N_t N_r}\left(\sum_{j=1}^{n}\sum_{i=1}^{n} \sqrt{\gamma_{v_i}} h_{v_i} G_r\left(\Omega_{\phi_{v_j}^r} - \Omega_{\phi_{v_i}^r}\right) G_t\left(\Omega_{\phi_{v_i}^t} - \Omega_{\phi_{v_i}^t}\right) s \right. \\ &\quad \left. + \sum_{j=1}^{n}\sum_{i=1}^{|\mathcal{T}^c|} \sqrt{\gamma_{l_i}} h_{l_i} G_r\left(\Omega_{\phi_{v_j}^r} - \Omega_{\phi_{l_i}^r}\right) G_t\left(\Omega_{\phi_{l_i}^t} - \Omega_{\theta_{l_i}^t}\right) s_{l_i}\right) + z,\end{aligned} \tag{8}$$

where $z = \mathbf{w}^* \mathbf{n} \sim \mathcal{C}N(0, \sigma_n^2)$, with $\sigma_n^2 = \sigma^2 \|\mathbf{w}\|^2$, and where we denoted the inner product $\mathbf{a}_x(\phi_1)^* \mathbf{a}_x(\phi_2) = G_x(\Omega_{\phi_1} - \Omega_{\phi_2})$, $x \in \{t, r\}$, by the antenna-array-gain function

$$\begin{aligned} G_x(y) &:= e^{j\pi\Delta_x(N_x-1)y} \frac{\sin(\pi \Delta_x N_x y)}{N_x \sin(\pi \Delta_x y)} \\ &: |G_x(y)| \le 1, \quad x \in \{t, r\}, \end{aligned} \tag{9}$$

with $\Omega_\phi := \cos(\phi)$ being the directional cosine and Δ_x, $x \in \{t, r\}$ the normalized antenna separation.

G. SINR Expression

Based on (8), the instantaneous SINR is then given by

$$\text{SINR} = \frac{\left|\sum_{i=1}^{n} \sqrt{\gamma_{v_i}} h_{v_i} C_{v_i}\right|^2}{\frac{\sigma_n^2}{N_t N_r} + \sum_{i=1}^{|\mathcal{T}^c|} \gamma_{l_i} |h_{l_i}|^2 |D_{l_i}|^2 \left|G_t(\Omega_{\phi_{l_i}^t} - \Omega_{\theta_{l_i}^t})\right|^2}, \tag{10}$$

where $C_{v_i} := \sum_{j=1}^{n} G_r(\Omega_{\phi_{v_j}^r} - \Omega_{\phi_{v_i}^r})$ and $D_{l_i} := \sum_{j=1}^{n} G_r(\Omega_{\phi_{v_j}^r} - \Omega_{\phi_{l_i}^r})$.

Assuming a single antenna receiver $N_r = 1$ (and thus $C_{v_i} = D_{l_i} = n$ and $\sigma_n^2 = n^2\sigma^2$), the SINR in (10) simplifies to

$$\text{SINR} = \frac{\left|\sum_{i=1}^{n} \sqrt{\gamma_{v_i}} h_{v_i}\right|^2}{\frac{\sigma^2}{N_t} + \sum_{i=1}^{|\mathcal{T}^c|} \gamma_{l_i} |h_{l_i}|^2 \left|G_t(\Omega_{\phi_{l_i}^t} - \Omega_{\theta_{l_i}^t})\right|^2}. \tag{11}$$

The coverage probability for the typical single-antenna user with SINR as in (11) will be derived under the assumption that all angles are independent and uniformly distributed between $[-\pi, +\pi]$. We will first assume that a signal cluster with many scatterers reach the receiver (Rayleigh fading assumption) and

that each tier experiences blockage. In this scenario the coverage probability is given in Theorem 1. The Nakagami fading distribution is then used to model the less severe fading distribution on the direct cooperating links and two upper bounds on the coverage probability are then derived and are given in Theorem 3 and Corollary 4. The case where there is no small scale fading for the direct cooperating links is then considered and the coverage probability for this case is given in Theorem 5. The exact coverage probability for the Nakagami(m) fading distribution could not be explicitly derived, but only an upper bound; therefore, by setting $m = 1$ and $m = \infty$ in the upper bound one can not obtain the exact coverage probabilities for the Rayleigh and no-fading cases in Theorems 1 and Theorem 5, respectively.

III. Coverage Probability With Rayleigh Fading

The main result of this section is:

Theorem 1: The coverage probability for the typical single antenna user in a downlink mmWave heterogenous network with K tiers, and where each tier has a blockage parameter β_k, with n base stations having ULA with N_t antennas, jointly transmitting to it is given by

$$\mathbb{P}(\text{SINR} > T) = \int\limits_{0<\kappa_1<\cdots<\kappa_n<+\infty} \mathcal{L}_{\text{I}}\left(\frac{T}{\sum_{i\le n}\kappa_i^{-1}}\right) \times \mathcal{L}_{\text{N}}\left(\frac{T}{\sum_{i\le n}\kappa_i^{-1}}\right) f_{\Gamma}(\kappa)d\kappa, \quad (12)$$

where $\kappa_i = \frac{\|v_i\|^{\alpha}}{P_{f(v_i)}}$, $i \in [1:n]$, refers to the random variable that denotes the inverse of the pathloss, the Laplace transform of the interference (I) and the noise (N) are respectively given by

$$\mathcal{L}_{\text{I}}(s) = \exp\left(-\int_{\kappa_n}^{\infty}\left[1-\int_{-2}^{+2}\left(\frac{1}{1+s|G_t(\varepsilon)|^2 v^{-1}}\right)f_{\Upsilon}(\varepsilon)d\varepsilon\right]\times\lambda(v)dv\right), \quad (13)$$

$$\mathcal{L}_{\text{N}}(s) = e^{-s\sigma^2/N_t}, \quad (14)$$

where the antenna array gain $G_t(\varepsilon)$ is given in (9), the probability density function of $\Upsilon_i = \Omega_{\phi_{l_i}^t} - \Omega_{\theta_{l_i}^t}$ is

$$f_{\Upsilon}(\varepsilon) = \int_{\max\{-1,-1-\varepsilon\}}^{\min\{1,1-\varepsilon\}}\left(\frac{1}{\pi^2\sqrt{1-(\varepsilon+y)^2}}\frac{1}{\sqrt{1-y^2}}\right)dy, \quad (15)$$

and $f_{\Gamma}(\kappa)$ is the joint distribution of $\kappa = [\kappa_1, \ldots, \kappa_n]$ and is given by

$$f_{\Gamma}(\kappa) = \prod_{i=1}^{n}\lambda(\kappa_i)e^{-\Lambda(\kappa_n)}, \quad (16)$$

while the intensity (λ) and intensity measure (Λ) are given by

$$\lambda(v) = \sum_{k=1}^{K} A_k v^{\frac{2}{\alpha_{\text{LOS}}}-1}e^{-a_k v^{\frac{1}{\alpha_{\text{LOS}}}}} + B_k v^{\frac{2}{\alpha_{\text{NLOS}}}-1}\left(1-e^{-b_k v^{\frac{1}{\alpha_{\text{NLOS}}}}}\right), \quad (17)$$

$$\Lambda(\kappa_n) = \sum_{k=1}^{K}\frac{2\pi\lambda_k}{\beta_k^2}\left(1-e^{-\beta_k(\kappa_n P_k)^{\frac{1}{\alpha_{\text{LOS}}}}}\left(1+\beta_k(\kappa_n P_k)^{\frac{1}{\alpha_{\text{LOS}}}}\right)\right) + \pi\lambda_k(\kappa_n P_k)^{\frac{2}{\alpha_{\text{NLOS}}}} - \frac{2\pi\lambda_k}{\beta_k^2} \times\left(1-e^{-\beta_k(\kappa_n P_k)^{\frac{1}{\alpha_{\text{NLOS}}}}}(1+\beta_k(\kappa_n P_k)^{\frac{1}{\alpha_{\text{NLOS}}}})\right), \quad (18)$$

$$A_k = \pi\lambda_k\frac{2}{\alpha_{\text{LOS}}}P_k^{\frac{2}{\alpha_{\text{LOS}}}}, \quad (19)$$

$$a_k = \beta_k P_k^{\frac{1}{\alpha_{\text{LOS}}}}, b_k = \beta_k P_k^{\frac{1}{\alpha_{\text{NLOS}}}}, \quad (20)$$

$$B_k = \pi\lambda_k\frac{2}{\alpha_{\text{NLOS}}}P_k^{\frac{2}{\alpha_{\text{NLOS}}}}. \quad (21)$$

Proof: Please refer to Appendix A for the proof. ■

The case of no blockage, as in microwave networks, can be obtained from Theorem 1 as follows:

Corollary 2: By setting the blockage parameters $\beta_k = 0$, $k \in [1:K]$, the coverage probability in Theorem 1 corresponds to the coverage probability in the absence of blockage. In this case the intensity and intensity measure in (17) and (18) simplify to

$$\lambda(v) = \sum_{k=1}^{K}\lambda_k\frac{2\pi}{\alpha_{\text{LOS}}}P_k^{\frac{2}{\alpha_{\text{LOS}}}}v^{\frac{2}{\alpha_{\text{LOS}}}-1}, \quad (22)$$

$$\Lambda(\kappa_n) = \sum_{k=1}^{K}\pi\lambda_k P_k\kappa_n^{\frac{2}{\alpha_{\text{LOS}}}}. \quad (23)$$

where α_{LOS} is the pathloss without blockage.

A. Numerical Results

Example 1: In this section we numerically evaluate Corollary 2. We compute the coverage probability for the typical user in a mmWave CoMP heterogenous network operating compliant with cellular systems operating at 28 GHz [8], and compare it to the case with no base station cooperation in the absence of blockage. The aim of this example is to understand the effect of cooperation with different number of transmit antennas. We consider a two tier network, $K = 2$, with parameters given in Table V. The noise variance is given by $\sigma^2(\text{dBm}) = -174 + 10\log_{10}(\text{BW}) + \text{NF (dB)}$, where BW and NF are abbreviations for bandwidth and noise figure, respectively. In Fig. 2 the coverage probability in (12) for $n = 2$ and $n = 1$ is plotted. This example shows that:

- In the absence of blockage, the increase in coverage probability with cooperation for the case of $N_t = 8, 16$ antennas is almost 11% at $T = 5$ dB. While the increase is 10% for $N_t = 32, 64$ at $T = 10$ dB.
- As expected, an increase in the number of antennas at the base stations increases the coverage probability. For example, for the same threshold $T = 10$ dB, the coverage probability with cooperation and with $N_t = 16$ is approximately 0.5 while for $N_t = 32$ is 0.65.
- The increase in coverage probability with cooperation decreases with an increase in number of antennas since

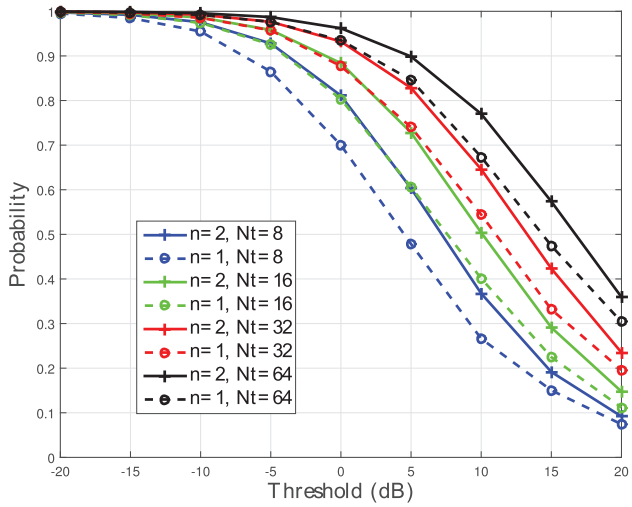

Fig. 2. Coverage probability in (12) for a two-tier network with parameters in Table V with two cooperating base stations ($n = 2$) and without base station cooperation ($n = 1$) and for different number of antennas.

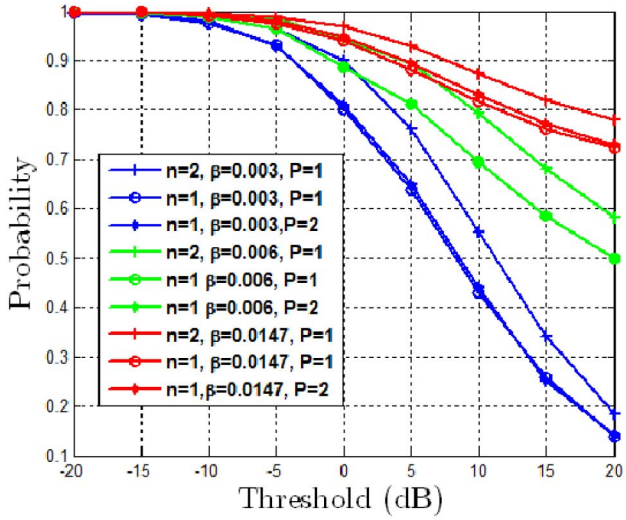

Fig. 3. Coverage probability in Theorem 1 for a one-tier network with parameters in Table V with two cooperating base stations ($n = 2$) and without base station cooperation ($n = 1$) and for different blockage parameters.

with higher directional transmission interference becomes limited and therefore the gain from cooperation is limited too.

Remark 2: The authors in [9] compare a two tier network with parameters (power, noise, intensities) suitable for microwave deployment with and without base station cooperation. An increase of 17% was noted at a threshold $T = 0$ dB for the case of CoMP with two cooperating base stations and single antenna receiver when compared to the case of no cooperation. We shall show that a comparable gain (16%-18%) to the one reported in [9] can be attained with two cooperating base stations with non fading channel gains in Section V. Thus, the Rayleigh fading assumption considered here provides a worse case scenario.

In the following examples we numerically evaluate Theorem 1 with blockage. The examples provided next illustrate scenarios when cooperation is beneficial (in terms of increasing the coverage probability) and examples when the increase is not substantial. Numerical results suggest that the former is in fact the case when the mmWave network is dense (captured by the tier radius and consequently its intensity) – a feature expected for millimeter wave networks [1], [7]. This can be interpreted as follows with extreme densification, the number of LOS interfering base stations increases and thus interference increases, a remark also noted in [7]. Therefore, cooperation limits the interference by increasing the number of serving base stations and therefore providing higher coverage probabilities.

Example 2: In Fig. 3 we plot the coverage probabilities for a single tier with parameters given in Table V. A tier with average radius of 80 m is considered with blockage parameters $\beta = 0.003, 0.006, 0.0143$ (corresponding to average LOS range which is greater than 80 m for $\beta = 0.003$, and an average range that cannot reach a user at the cell edge for $\beta = 0.0143$). The coverage probability for this one tier CoMP mmWave network with $n = 2$ and with base station power available $P = 1W$ is compared with the following cases: Case 1) a one tier mmWave network with no base station cooperation ($n = 1$), with a base station transmit power $P = 1$ W; Case 2) a one tier mmWave network with no base station cooperation $n = 1$, but with base station transmit power equal to the sum of transmit power if two base stations were to cooperate $P = 2$ W. This example shows that:

- The increase in coverage probability for both cases is approximately an increase of 0.12 in probability for a threshold $T = 5, 10$ dB.
- Moreover, it is interesting to note that an increase in the tier blockage parameter (shorter range of LOS links) increases the coverage probability. This can be interpreted as follows: an increase in the blockage parameter increases the probability of blockage of the interfering LOS base stations, resulting in higher coverage probabilities. The curves corresponding to the coverage probabilities to Case 1 and Case 2 are very close since the power at the interfering base stations has also increased with this assumption (which also means that this network is not noise limited).

We shall show in the subsequent example, that this observation does not hold for a less dense (large average cell radius) tier with a high probability of NLOS base stations.

Example 3: A tier with an average radius of 250 m and with tier parameters given in Table V and with a blockage parameter $\beta = 0.02$ (corresponding to a high probability of blockage and average LOS range of 50 m) is plotted in Fig. 4. This example shows that:

- The increase in coverage probability due to cooperation in this case is minimal and is approximately 0.05 at all thresholds. This can be interpreted as follows: 1) a tier with high blockages will also block interfering signals, and 2) when the density of base stations is not too dense, the n strongest base stations are not *too strong* to cause a substantial increase in coverage probability due to the fact that distance at which these cooperating base stations are located increases too (thus received power decreases).

TABLE V
TIER PARAMETERS FOR FIGS. 2, 3, 4, 5

Parameter	Example 1, Fig. 2	Example 2, Fig. 3	Example 3, Fig. 4	Example 4, Fig. 5
Intensity	$\lambda_1 = (150^2\pi)^{-1}, \lambda_2 = (50^2\pi)^{-1}$	$\lambda_1 = (80^2\pi)^{-1}$	$\lambda_1 = (250^2\pi)^{-1}$	$\lambda_1 = (50^2\pi)^{-1}$
Power	$P_1 = 1$W, $P_2 = 0.25$W	$P_1 = 1$W	$P_1 = 1$W	$P_1 = 1$W
Path Loss	$\alpha_{\text{LOS}} = 3$	$\alpha_{\text{LOS}} = 2, \alpha_{\text{NLOS}} = 4$	$\alpha_{\text{LOS}} = 2, \alpha_{\text{NLOS}} = 4$	$\alpha_{\text{LOS}} = 2, \alpha_{\text{NLOS}} = 4$
Antennas	$N_t = 8, 16, 32, 64$	$N_t = 16$	$N_t = 64$	$N_t = 64$
Noise Figure	10dB	5dB	5dB	10dB
Blockage	$\beta = 0$	$\beta = 0.003, 0.006, 0.0143$	$\beta = 0.02$	$\beta = 0.004$
Bandwidth	1GHz	1GHz	1GHz	1GHz

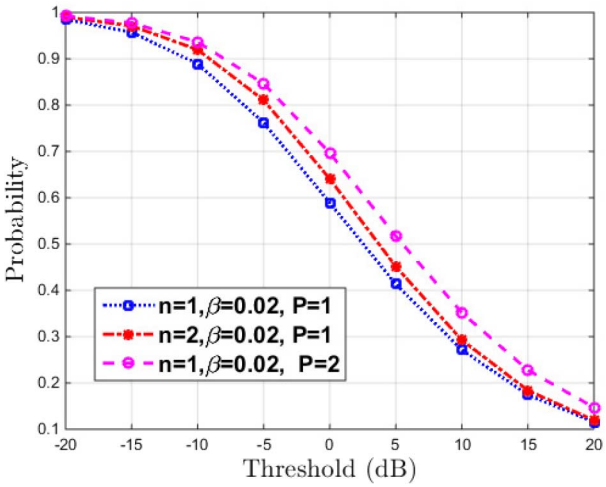

Fig. 4. Coverage probability in Theorem 1 for a one-tier network with parameters in Table V with two cooperating base stations ($n = 2$) and without base station cooperation ($n = 1$).

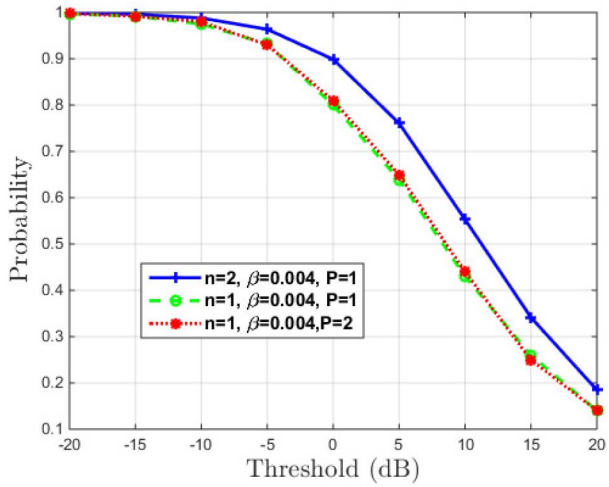

Fig. 5. Coverage probability in Theorem 1 for a one-tier network with parameters in Table VI with two cooperating base stations ($n = 2$) and without base station cooperation ($n = 1$).

- As seen in Fig. 4, increasing the power at the base station (but no cooperation) provides higher coverage probability than the case with base station cooperation. We shall show that the observations made for this example do not hold when there is no fading on the direct links from the cooperating base stations in Section V.

Example 4: In an attempt to understand whether the observations (relatively smaller cell radii tier benefit from base station cooperation more) hold for a network that is not noise limited as in Example 2 but for a larger number of antennas at the base stations, we consider the example of a dense mmWave tier network (average radius of 50 m) and $N_t = 64$ and with network parameters as in Table V. In Fig. 5 we plot the coverage probabilities corresponding for the different cases which are described in Example 2. The observations made in Example 2 hold for this example too with almost the same increase (11%) in coverage probability for a threshold $T = 10, 15$ dB.

IV. COVERAGE PROBABILITY WITH NAKAGAMI FADING

In this section we consider the same network model described in Section II but choose a different fading distribution on the channel gains from the strongest cooperating base stations, similar to [4]. In particular we consider Nakagami fading with parameter m, while keeping the same assumption of Rayleigh fading for the interfering channel gains. By using the coverage probability expression for a general fading distribution [16, Eq. 2.11], we are then able to derive an upper bound (since an upper bound on the strength of the desired signal has been considered) on the coverage probability for this network. We then consider another upper bound by evaluating the network in the absence of interference. The main result of this section is as follows

Theorem 3: An upper bound on the coverage probability for the single antenna typical user in a downlink mmWave heterogenous network with blockage with K tiers, where each tier has a blockage parameter β_k, and with n base stations having ULA with N_t antennas jointly transmitting to it, with the assumption of Nakagami(m) fading on the cooperating channel gains is

$$\mathbb{P}(\text{SINR} > T) \leq \int_{0<\kappa_1<\cdots<\kappa_n<+\infty} f_\Gamma(\kappa) \int_{-\infty}^{\infty} \mathcal{L}_{\text{I}}(2j\pi T's) \times \mathcal{L}_{\text{N}}(2j\pi T's) \frac{\mathcal{L}_S^{\text{UP}}(-2j\pi s) - 1}{2j\pi s} ds\, d\kappa, \tag{24}$$

where $T' := \frac{T}{\sum_{i\leq n} \kappa_i^{-1}}$, $\kappa_i = \frac{\|v_i\|^\alpha}{P_{f(v_i)}}$, $i \in [1:n]$, refers to the random variable that denotes the inverse of the pathloss, and the joint distribution of $\kappa = [\kappa_1, \cdots, \kappa_n]$ is given by (16), where the Laplace transform of the interference (I) (by assuming Rayleigh fading on the interfering links) is given by (13) and the Laplace transform of the noise (N) is given by (14), the intensity and intensity measure are given by (17) and (18),

TABLE VI
TIER PARAMETERS FOR FIGS. 6, 7(A), 7(B)

Parameter	Example 5, Fig. 6	Example 6, Fig. 7(a)	Example 6, Fig. 7(b)
Intensity	$\lambda_1 = (200^2\pi)^{-1}$	$\lambda_1 = (200^2\pi)^{-1}$	$\lambda_1 = (80^2\pi)^{-1}$
Power	$P_1 = 1$W	$P_1 = 1$W	$P_1 = 1$W
Path Loss	$\alpha_{\text{LOS}} = 2, \alpha_{\text{NLOS}} = 4$	$\alpha_{\text{LOS}} = 2, \alpha_{\text{NLOS}} = 4$	$\alpha_{\text{LOS}} = 2, \alpha_{\text{NLOS}} = 4$
Antennas	$N_t = 16$	$N_t = 64$	$N_t = 16$
Noise Figure	5dB	5dB	5dB
Blockage	$\beta = 0.025$	$\beta = 0.025$	$\beta = 0.003$
Bandwidth	1GHz	1GHz	1GHz

respectively, and where the Laplace transform for the upper bound on intended signal is given by

$$\mathcal{L}_{\text{S}}^{\text{UP}}(s) = \frac{1}{(1+s/m)^{nm}}. \tag{25}$$

Proof: The main idea is to upper bound the true signal $S = |\sum_{i=1}^{n} \sqrt{\gamma_{v_i}} h_{v_i}|^2$ with its 'coherent combined' version $S^{\text{UP}} = \sum_{i=1}^{n} \gamma_{v_i} |h_{v_i}|^2$. This has been done as a closed form expression for the distribution of S is not available, to the best of our knowledge. The distribution is exact if $n = 1$.

Please refer to Appendix B for a detailed proof. ■

Next, we consider another upper bound, given in Corollary 4, on the coverage probability with Nakagami fading presented in Theorem 4. In this bound, we still coherently combine the direct link gains, as in Theorem 3, but in addition we neglect the interference term by setting $\mathcal{L}_{\text{I}}(s) = 1$. The two upper bounds are expected to give almost equal coverage probabilities in noise limited networks where indeed interference is negligible. We will show that this in fact the case, by a numerical example later on.

Corollary 4: Under the same assumptions and with the same notation convention as in Theorem 3, an upper bound on the coverage probability in the absence of interference is

$$\mathbb{P}(\text{SNR} > T) \leq \int_{0<\kappa_1<\cdots<\kappa_n<+\infty} f_{\Gamma}(\kappa) \left(\frac{g^{(nm-1)}\left(\frac{m}{2\pi j}\right)}{(nm-1)!} \right) d\kappa. \tag{26}$$

$$g(z) = (-1)^{nm} \frac{1 - \left(1 - \frac{2\pi j z}{m}\right)^{nm}}{\left(\frac{2\pi j}{m}\right)^{nm} (2\pi j z)} e^{-2\pi j z \frac{T'\sigma^2}{N_t}}, \tag{27}$$

and where $g^{(i)}(z)$ is the $i-th$ derivative of the function $g(z)$.

Proof: Please refer to Appendix B for the proof. ■

Before moving to numerical examples to exemplify the performance with Nakagami fading, we would like to point out that for the case without base station cooperation, that is $n = 1$, the coverage probabilities in (24) and (26) are exact (i.e., not an upper bound).

A. Numerical Results

Example 5: We consider a one tier network with two cooperating base stations and with tier parameters given in Table VI. The coverage probability in (24) for the case of $m = 3$ with and without base station cooperation are plotted. The purpose of this numerical example is to show that for tiers with high probability of blockage, in this case taken to be $\beta = 0.025$ (corresponding to a high probability of blockage and average LOS range of 40 m), evaluation of the coverage probability of the network with and without the absence of interference yields almost exact numerical results. Therefore, we fix $n = 2$ and we plot the coverage probability in (24) and (26) for: Case 1) $m = 3$ and $n = 2$. We use Theorem 1 to plot the coverage probability for the Rayleigh fading; Case 2) $m = 1$ and $n = 2$ (also with and without interference). The two curves shown in Fig. 6 for each of the cases corresponding to the Rayleigh and Nakagami fading almost exactly overlap. Therefore, we have the following conclusions:

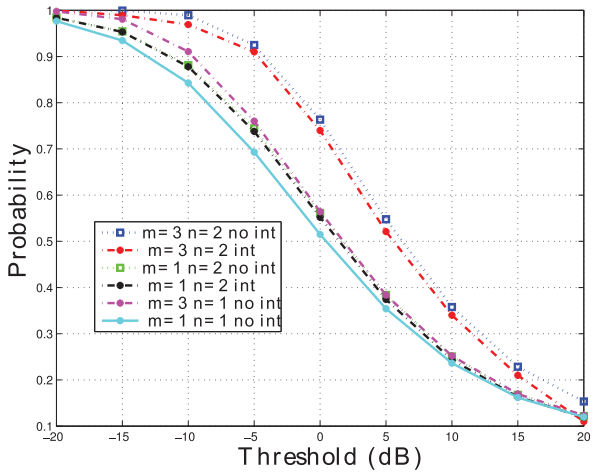

Fig. 6. Upperbounds on coverage probability in Theorem 3 and Corollary 4 for a one tier network with parameters in Table VI and for $n = 2$ (two cooperating base stations) and for $n = 1$ (no CoMP). The lower bounds are plotted using Theorem 1.

- The exact coverage probability with cooperation ($n = 2$) and with Nakagami fading distributed desired links lies in between the upper bound (red) and the lower bound (black).
- For mmWave networks with high blockage, the network is noise limited (blue and red curves are almost overlapping in Fig. 6), therefore the probability that the SNR (as opposed to SINR) is greater than a non-negative threshold ($\mathbb{P}(\text{SNR} > T)$) is almost equal to the $\mathbb{P}(\text{SINR} > T)$.
- For the case with no CoMP, $n = 1$, coverage (exact and not upper bound) is at most 6% higher when Nakagami fading with parameter $m = 3$ is considered as compared to the Rayleigh fading on the desired links (cyan and magenta curves in Fig. 6).

V. Coverage Probability Without Small Scale Fading

In this section we consider the same network model as in Section II but where the cooperating channel gains do not experience any fading. As shown in [17], the assumption of having no small scale fading from the serving base stations is a good assumption in mmWave systems due to the highly directional transmission and when the receivers are not present in a rich scattering environment (in rich scattering environments Rayleigh fading may be more reasonable). The Rayleigh distribution is used to model the fading distribution of the interfering channel gains. Interestingly, we will show through numerical examples that the increase in coverage probability with two cooperating base stations is more pronounced when the cooperating channels experience no fading than that obtained when the fading is assumed to be the Rayleigh fading.

Theorem 5: The coverage probability in the absence of small scale fading for the typical single antenna user in a downlink mmWave heterogenous network with blockage with K tiers, where each tier has a blockage parameter β_k, and with n base stations having ULA with N_t antennas jointly transmitting to it, with the assumption of no fading on the cooperating channel gains is

$$\mathbb{P}(\text{SINR} > T) = \int\limits_{0<\kappa_1<\cdots<\kappa_n<+\infty} f_\Gamma(\kappa) \int_{-\infty}^{\infty} \mathcal{L}_\text{I}(2j\pi Ts) \times \mathcal{L}_\text{N}(2j\pi Ts) \frac{\mathcal{L}_S(-2j\pi s)-1}{2j\pi s} ds\, d\kappa, \quad (28)$$

where $\kappa_i = \frac{\|v_i\|^\alpha}{P_{f(v_i)}}$, $i \in [1:n]$, refers to the random variable that denotes the inverse of the pathloss and the joint distribution of $\kappa = [\kappa_1, \ldots, \kappa_n]$ is given by (16) with an intensity and intensity measure as in (17) and (18), respectively, and where $\mathcal{L}_\text{S}(s) = e^{-s(\sum_{i\le n}\kappa_i^{-1/2})^2}$ and $\mathcal{L}_\text{N}(s) = e^{-s\sigma^2/N_t}$.

Proof: The proof follows easily from finding the Laplace transform of the desired signal and is thus omitted for sake of space. ■

A. Numerical Results

Example 6: In this example we numerically evaluate Theorem 5. We consider a one tier network with tier parameters given in Table VI. The coverage probability in Theorem 5 with two cooperating base stations is plotted against the two different cases described as in Example 2. We also plot the three curves corresponding to the Rayleigh fading assumption on the cooperating channel gains in Theorem 1. The curves in Fig. 7(a) suggest that:

- The increase in coverage probability with CoMP is mainly due to a power increase since the curve corresponding to the case when there is no CoMP but with double transmit power is very close to that of the curve of having two cooperating base stations but with half the transmit power. This also implies that this network is noise limited. This observation is valid for the networks where gains from cooperating base stations are non fading or when they are Rayleigh fading.

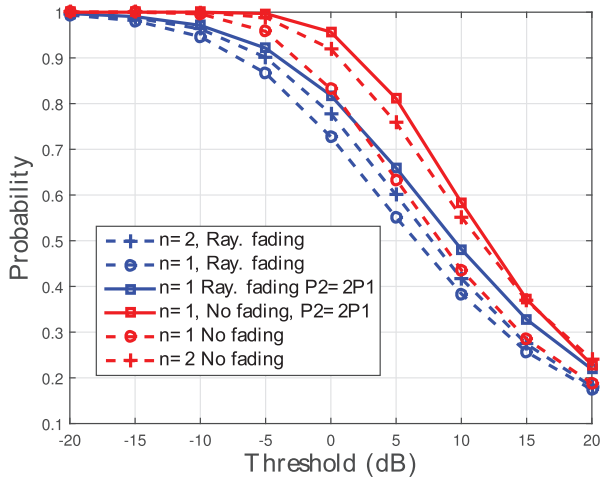

(a) Coverage probability for a one tier network with parameters in Table VI.

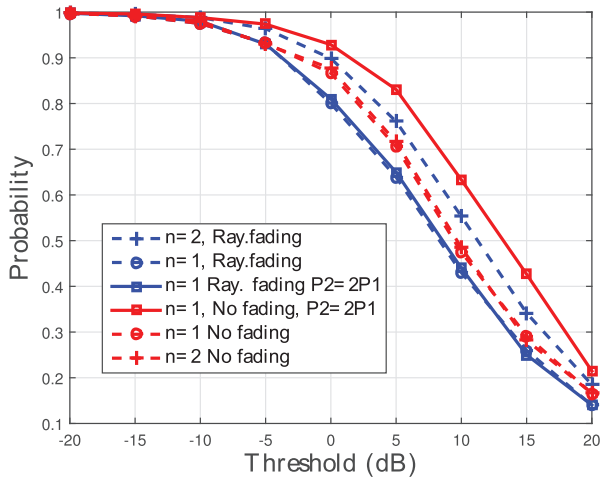

(b) Coverage probability for a one tier network with parameters in Table V (Example 2) $\beta = 0.003$.

Fig. 7. Plots of coverage probabilities in Theorem 5 for noise and interference limited networks with two cooperating base stations ($n = 2$) and with no CoMP ($n = 1$). The coverage probabilities for the same network parameters but with Rayleigh assumption in Theorem 1 are also plotted for ($n = 1$) and ($n = 2$).

- It is interesting to note that the increase in probability with two cooperating base stations (almost 18% for threshold $T = 5$ dB) for the case when there is no small scale fading exceeds the increase with CoMP (5% for the same threshold) for the case when the channel gains are Rayleigh distributed and hence implying that CoMP provides larger gains for mmWave networks with no small scale fading from the serving base stations.

Example 7: In an attempt to understand whether the observations made in Example 6 hold for a network which is not noise limited, we consider the network in Example 2 ($\beta = 0.003$) and compare the Rayleigh fading case to the case when there is no small scale fading. In Fig. 7(b) we plot the curves corresponding to the different cases as explained in Example 2 along with the curves corresponding to the coverage probabilities non fading networks in Theorem 5. The increase in coverage probability with CoMP ($n = 2$) is an increase of 16% at threshold $T = 10$, while the increase with CoMP for the Rayleigh fading case is almost 12% at the same threshold.

VI. Conclusions

In this paper we considered the problem of base station cooperation in mmWave heterogenous networks. Using stochastic geometry, coverage probabilities were derived at the typical user, accounting for directionality at the base stations, blockage, interference and different fading distributions. Numerical results suggest that coverage with CoMP rival that with no CoMP especially in dense mmWave networks with no small scale fading on the cooperating channel gains. Future work includes deriving the coverage probability at a multi-antenna typical receiver and accounting for possible errors due to beam steering. Characterizing the rate tradeoff with the increase in load (number of served receivers) on each mmWave base station with base station cooperation, incorporating different fading distributions for LOS and NLOS links and re-assessing the mmWave network accordingly are part of ongoing investigation.

APPENDIX A
Proof of Theorem 1

The analysis of the coverage probability for the mmWave heterogeneous network is similar to that in [9, Appendix A] with three major differences. The first difference is the presence of multiple antennas at the transmitter. The second difference is that the interference is a function of i.i.d uniformly distributed random variables, assuming that the path angles are independent and uniformly distributed over $[-\pi, +\pi]$. The third difference is blockage that makes the pathloss exponent a random variable.

Let $\Theta_k = \{\frac{\|v\|^{\alpha}}{P_k}, v \in \Phi_k\}$ for $k \in [1:K]$ with intensity $\lambda_k(v)$. The pathloss α is a random variable that takes on values α_{LOS} and α_{NLOS} with probability $e^{-\beta_k v}$ and $1 - e^{-\beta_k v}$ respectively (note that we have dropped the $\|.\|$ of v for easier notation). Then the process $\Theta = \cup_{k=1}^{K} \Theta_k$ is a non-homogenous PPP with density $\lambda(v) = \sum_{k=1}^{K} \lambda_k(v)$. In the following we compute the intensity and intensity measure of Θ_k for $k \in [1:K]$. By using the Mapping Theorem [18, Thm. 2.34] the intensity measure and the intensity of each tier k, $k \in [1:K]$, are given by

$$\begin{aligned}\Lambda_k([0,r]) &= \int_0^{(rP_k)^{\frac{1}{\alpha_{\text{LOS}}}}} 2\pi\lambda_k v e^{-\beta_k v} dv \\ &\quad + \int_0^{(rP_k)^{\frac{1}{\alpha_{\text{NLOS}}}}} 2\pi\lambda_k v \left(1 - e^{-\beta_k v}\right) dv \\ &= \frac{2\pi\lambda_k}{\beta_k^2}\left(1 - e^{-\beta_k (rP_k)^{\frac{1}{\alpha_{\text{LOS}}}}}\left(1 + \beta_k (rP_k)^{\frac{1}{\alpha_{\text{LOS}}}}\right)\right) \\ &\quad + \pi\lambda_k (rP_k)^{\frac{1}{\alpha_{\text{NLOS}}}} \\ &\quad - \frac{2\pi\lambda_k}{\beta_k^2}\left(1 - e^{-\beta_k (rP_k)^{\frac{1}{\alpha_{\text{NLOS}}}}}\left(1 + \beta_k (rP_k)^{\frac{1}{\alpha_{\text{NLOS}}}}\right)\right),\end{aligned} \tag{29}$$

$$\begin{aligned}\lambda_k(v) &= \frac{d\Lambda_k([0,v])}{dv} = A_k v^{\frac{2}{\alpha_{\text{LOS}}}-1} e^{-a_k v^{\frac{1}{\alpha_{\text{LOS}}}}} \\ &\quad + B_k v^{\frac{2}{\alpha_{\text{NLOS}}}-1}\left(1 - e^{-b_k v^{\frac{1}{\alpha_{\text{NLOS}}}}}\right),\end{aligned} \tag{30}$$

with

$$\begin{aligned}A_k &= \pi\lambda_k \frac{2}{\alpha_{\text{LOS}}} P_k^{\frac{2}{\alpha_{\text{LOS}}}}, \\ a_k &= \beta_k P_k^{\frac{1}{\alpha_{\text{LOS}}}}, \\ b_k &= \beta_k P_k^{\frac{1}{\alpha_{\text{NLOS}}}} \text{ and} \\ B_k &= \pi\lambda_k \frac{2}{\alpha_{\text{NLOS}}} P_k^{\frac{2}{\alpha_{\text{NLOS}}}}.\end{aligned}$$

A. Distribution of Strongest Base Stations

We assume that the elements in the process Θ are indexed in increasing order. Let $\kappa_i = \frac{\|v_i\|^{\alpha}}{P_{f(v_i)}}$ then $\kappa = \{\kappa_1, \ldots, \kappa_n\}$ denotes the set of *inverse of the pathloss* of the cooperating base stations. We first present the distribution of the two nearest base stations by following similar steps as done in [19], then derive the distribution of the n closest base stations. The distribution of the closest two base stations (assuming two cooperating base stations) is given by

$$f_{\Gamma}(\kappa_1, \kappa_2) = f_{\Gamma_2'|\Gamma_1'}(\kappa_2|\kappa_1)\, f_{\Gamma_1'}(\kappa_1), \tag{31}$$

where the distribution of the first base station with strong received power is obtained from the null probability of a PPP and is given by

$$f_{\Gamma_1'}(\kappa_1) = \lambda(\kappa_1) e^{-\Lambda(\kappa_1)}, \tag{32}$$

while the conditional distribution is given by

$$f_{\Gamma_2'|\Gamma_1'}(\kappa_2|\kappa_1) = \lambda(\kappa_2) e^{-\Lambda(\kappa_2)+\Lambda(\kappa_1)}. \tag{33}$$

The joint distribution for the case of $n = 2$ base stations is obtained by substituting (32) and (33) in (31). The result can be generalized to any number n of cooperating base stations

$$f_{\Gamma}(\kappa) = \prod_{i=1}^{n} \lambda(\kappa_i) e^{-\Lambda(\kappa_n)}. \tag{34}$$

B. Derivation of Coverage Probability

We have assumed that the cooperating base stations have *inverse of pathloss* κ_i by $i \leq n$, then the desired signal power at the numerator of (11) can be re-written as

$$S = \left|\sum_{i=1}^{n} \sqrt{\gamma_{v_i}} h_{v_i}\right|^2 = \left|\sum_{i \leq n} \kappa_i^{-1/2} h_i\right|^2.$$

We have that the interfering base stations are indexed with $i > n$, then the power of the interference I can be expressed (by replacing the index l_i with just i) as

$$\begin{aligned}I &= \sum_{i=1}^{|\mathcal{T}|^c} \gamma_{l_i} |h_{l_i}|^2 \left|G_t\left(\Omega_{\phi_{l_i}^t} - \Omega_{\theta_{l_i}^t}\right)\right|^2 \\ &= \sum_{i>n} \kappa_i^{-1} |h_i|^2 \left|G_t(\Upsilon_i)\right|^2,\end{aligned} \tag{35}$$

The coverage probability for a threshold T, can be re-written

$$\begin{aligned}\mathbb{P}(\text{SINR} > T) &= \mathbb{P}\left(S > T(I + \frac{\sigma^2}{N_t})\right)\\ &= \mathbb{E}_{\kappa,I}\left[\mathbb{P}\left(\left|\sum_{i\le n}\kappa_i^{-1/2}h_i\right|^2 > T(I+\frac{\sigma^2}{N_t})\,\middle|\,\kappa, I\right)\right]\\ &\overset{(a)}{=} \mathbb{E}_{\kappa,I}\left[\exp\left(\frac{-T(I+\frac{\sigma^2}{N_t})}{\sum_{i\le n}\kappa_i^{-1}}\right)\right]\\ &\overset{(b)}{=} \mathbb{E}_{\kappa}\left[\mathcal{L}_{\mathrm{I}}\left(\frac{T}{\sum_{i\le n}\kappa_i^{-1}}\right)\mathcal{L}_{\mathrm{N}}\left(\frac{T}{\sum_{i\le n}\kappa_i^{-1}}\right)\right]\\ &\overset{(c)}{=} \int\limits_{0<\kappa_1<\cdots<\kappa_n<+\infty}\mathcal{L}_{\mathrm{I}}\left(\frac{T}{\sum_{i\le n}\kappa_i^{-1}}\right)\\ &\quad\times\mathcal{L}_{\mathrm{N}}\left(\frac{T}{\sum_{i\le n}\kappa_i^{-1}}\right)f_{\Gamma}(\kappa)d\kappa.\end{aligned}$$

where (a) follows from the cumulative density function of the exponentially distributed random variable S (due to Rayleigh fading assumption) with mean $\sum_{i\le n}\kappa_i^{-1}$; (b) follows from the definition of the Laplace transform of I, $\mathcal{L}_{\mathrm{I}}(s) = \mathbb{E}[e^{-sI}]$ and the Laplace transform of the noise, $\mathcal{L}_{\mathrm{N}}(s) = \mathbb{E}[e^{-s\sigma^2/N_t}]$; (c) by definition of the expectation with respect to the distribution of κ.

Next we evaluate the Laplace transform of the interference I in (35), but before going into the details of the derivation we need to find the distribution of $\Upsilon_i := \Omega_{\phi^t_{l_i}} - \Omega_{\theta^t_{l_i}}$, since the interference in (35) is a function of the beam forming gain function which in turn is a function of Υ_i. The beam forming gain is given by (9).

With the assumption that the interfering path angles of departure and the beam steering angle used by the interfering base stations are i.i.d $\sim U([-\pi, +\pi])$, then the directional cosine $\Omega_{\phi^t_{l_i}}$ and $\Omega_{\theta^t_{l_i}}$ are random variables with the following common probability density function

$$f_{\Omega}(\omega) = \begin{cases}\frac{1}{\pi\sqrt{1-\omega^2}} & \text{if } -1\le\omega\le 1;\\ 0 & \text{otherwise.}\end{cases}$$

then the distribution of $\Upsilon_i = \Omega_{\phi^t_{l_i}} - \Omega_{\theta^t_{l_i}}$ is the result of the convolution of the probability density functions of $\Omega_{\phi^t_{l_i}}$ and $\Omega_{\theta^t_{l_i}}$ and is given by

$$f_{\Upsilon_i}(\varepsilon_i) = \int_{\max\{-1,-1-\varepsilon_i\}}^{\min\{1,1-\varepsilon_i\}}\left(\frac{1}{\pi^2\sqrt{1-(\varepsilon_i+\omega)^2}}\frac{1}{\sqrt{1-\omega^2}}\right)dy. \tag{36}$$

Then the Laplace transform of the interference can be derived

$$\begin{aligned}\mathcal{L}_{\mathrm{I}}(s) &= \mathbb{E}\left[e^{-s\sum\limits_{i>n}\kappa_i^{-1}|h_i|^2|G_t(\Upsilon_i)|^2}\right]\\ &= \mathbb{E}\left[\prod_{i>n}\left(e^{-s\kappa_i^{-1}|h_i|^2|G_t(\Upsilon_i)|^2}\right)\right]\\ &\overset{(a)}{=} \mathbb{E}_{\{\Upsilon_i\},\Theta}\left[\prod_{i>n}\mathbb{E}_{|h|^2}\left(e^{-s\kappa_i^{-1}|h|^2|G_t(\Upsilon_i)|^2}\right)\right]\\ &\overset{(b)}{=} \mathbb{E}_{\{\Upsilon_i\},\Theta}\left[\prod_{i>n}\left(\frac{1}{1+s|G_t(\Upsilon_i)|^2\kappa_i^{-1}}\right)\right]\\ &\overset{(c)}{=} \mathbb{E}_{\Theta}\left[\prod_{i>n}\mathbb{E}_{\Upsilon}\left(\frac{1}{1+s|G_t(\Upsilon)|^2\kappa_i^{-1}}\right)\right]\\ &\overset{(d)}{=} \mathbb{E}_{\Theta}\left[\prod_{i>n}\left(\int_{-2}^{+2}\left(\frac{1}{1+s|G_t(\varepsilon)|^2\kappa_i^{-1}}\right)f_{\Upsilon}(\varepsilon)\,d\varepsilon\right)\right]\\ &\overset{(e)}{=} \exp\left(-\int_{\kappa_n}^{\infty}\left[1-\int_{-2}^{+2}\left(\frac{1}{1+s|G_t(\varepsilon)|^2v^{-1}}\right)f_{\Upsilon}(\varepsilon)d\varepsilon\right]\right.\\ &\quad\left.\times\,\lambda(v)\,dv.\right.\end{aligned} \tag{37}$$

where (a) follows from the i.i.d distribution of $|h_i|^2$ and their independence from Θ and Υ_i; (b) follows from the Rayleigh fading assumption and the moment generating function of an exponential random variable; (c) follows from the i.i.d distribution of Υ_i and their independence from Θ; (d) from the taking the expectation with respect to the random variable Υ_i whose distribution is given by (36); (e) follows from the probability generating function of poisson point process [18, Thm. 4.9] (as used in [10, Eq. (38)]) and where $\lambda(v)$ is given by (30).

Next we give an approximation of the Laplace transform of the interference for easier numerical evaluations (by approximating the beam forming gain function by a piecewise linear function) and to compare our results with [10], the Laplace transform of the interference is

$$\begin{aligned}\mathcal{L}_{\mathrm{I}}(s) &= \mathbb{E}_{\Theta}\left[\prod_{i>n}\left(\int_{-2}^{+2}\left(\frac{1}{1+s|G_t(\varepsilon)|^2\kappa_i^{-1}}\right)f_{\Upsilon}(\varepsilon)\,d\varepsilon\right)\right]\\ &\overset{(e)}{\approx} \mathbb{E}_{\Theta}\left[\prod_{i>n}\left(\int_{-2}^{-1/A_l}f_{\Upsilon}(\varepsilon)\,d\varepsilon + \int_{-1/A_l}^{1/A_l}\frac{1}{1+s\kappa_i^{-1}}f_{\Upsilon}(\varepsilon)\,d\varepsilon\right.\right.\\ &\quad\left.\left.+\int_{1/A_l}^{2}f_{\Upsilon}(\varepsilon)\,d\varepsilon\right)\right]\\ &\overset{(f)}{=} \mathbb{E}_{\Theta}\left[\prod_{i>n}\left(1-\frac{c\,s\gamma_i^{-1}}{1+s\gamma_i^{-1}}\right)\right]\\ &\overset{(g)}{=} \exp\left(-\int_{\kappa_n}^{\infty}\left[\frac{c\,sv^{-1}}{1+sv^{-1}}\right]\lambda(v)\,dv\right).\end{aligned}$$

where in (e) an approximation of the gain function was used which is given

$$G_t(\varepsilon) = \begin{cases}1 & \text{if } -\frac{1}{A_t}\le\varepsilon\le\frac{1}{A_l}, \quad , A_t = N_t\Delta_t\\ 0 & \text{if otherwise}\end{cases}; \tag{38}$$

(f) defining $c := \int_{-1/A_t}^{+1/A_t} f_{\Upsilon}(\varepsilon)\,d\varepsilon$; (g) follows from the probability generating function of poisson point process [18, Thm. 4.9] (as used in [10, Eq. (38)]) and where $\lambda(v)$ is given by (30).

Remark 3: If $c = 1$ then the Laplace transform in step (g) simplifies to that in [10, Eq. (38)].

Remark 4: A more accurate antenna gain function should account for the side lobe gain which is ideally non-zero, such as cone plus sphere model [20]. The approximation in (38) is a good approximation for an array with large number of antenna elements.

APPENDIX B
PROOF OF THEOREM 3 AND COROLLARY 4

C. Proof of Theorem 3

Let us re-consider a different distribution on the direct links - while keeping the same Rayleigh fading assumption on the interfering links - in particular let us consider that the fading is Nakagami with shape parameter m and scale parameter $\theta = 1$. In this case we will derive the distribution of an upper bound on the desired signal in particular the distribution of

$$S = \left| \sum_{i \leq n} \kappa_i^{-1/2} h_i \right|^2 \leq \sum_{i \leq n} \kappa_i^{-1} \sum_{i \leq n} |h_i|^2 = S^{\mathrm{UP}},$$

where

$$\mathbb{P}\left(S^{\mathrm{UP}} \geq T(I + \frac{\sigma^2}{N_t}) \right) = \mathbb{P}\left(\sum_{i \leq n} |h_i|^2 \geq \frac{T(I + \frac{\sigma^2}{N_t})}{\sum_i \gamma_i^{-1}} \right) = \mathbb{P}\left(S^{\mathrm{UP}} \geq T' \left(I + \frac{\sigma^2}{N_t} \right) \right),$$

where $T' = \frac{T}{\sum_i \gamma_i^{-1}}$, $S^{\mathrm{UP}} = \sum_i |h_i|^2$. The distribution of the upper bound and its Laplace transform are respectively given by

$$\sum_{i \leq n} |h_i|^2 \sim \Gamma(nm, 1/m) \leftrightarrow \mathcal{L}_{S^{\mathrm{UP}}}(s) = \frac{1}{(1 + s/m)^{nm}}.$$

We then have from [16, Eq. 2.11] that

$$\mathbb{P}\left(\mathrm{SINR} > T\right) = \mathbb{P}\left(S > T'(I + \frac{\sigma^2}{N_t}) \right) = \int_{0 < \kappa_1 < \cdots < \kappa_n < +\infty} f_\Gamma(\kappa) \times \int_{-\infty}^{\infty} \mathcal{L}_{\mathrm{I}}(2j\pi T' s) \mathcal{L}_{\mathrm{N}}(2j\pi T' s) \frac{\mathcal{L}_{S^{\mathrm{UP}}}(-2j\pi s) - 1}{2j\pi s} ds \, d\kappa,$$

where the joint distribution of κ is given by (34). Next we have from (37) the Laplace transform of the interference $\mathcal{L}_{\mathrm{I}}(s)$ with an intensity $\lambda(v)$ given by (30) while the Laplace transform of the noise is given by $\mathcal{L}_{\mathrm{N}}(s) = \mathbb{E}[e^{-s\frac{\sigma^2}{N_t}}] = e^{-s\frac{\sigma^2}{N_t}}$.

D. Proof of Corollary 4

The coverage probability in the absence of interference is given by (24) with $\mathcal{L}_{\mathrm{I}}(s) = 1$ is $\mathbb{P}(\mathrm{SNR} > T) =$

$$\int_{0 < \kappa_1 < \cdots < \kappa_n < +\infty} f_\Gamma(\kappa) \int_{-\infty}^{\infty} \frac{\frac{1}{(1 - \frac{2j\pi s}{m})^{nm}} - 1}{2j\pi s} e^{-2j\pi s \frac{T'\sigma^2}{N_t}} ds \, d\kappa \tag{39a}$$

$$= \int_{0 < \kappa_1 < \cdots < \kappa_n < +\infty} f_\Gamma(\kappa) \underbrace{\int_{-\infty}^{\infty} f(s) \, ds}_{Q} \, d\kappa. \tag{39b}$$

In the following we seek to solve Q. Note that a pole of order nm exists in the integrand thus the integral Q can be solved using contour integration and its Residue (Res) is

$$Q = \mathrm{Res}_{z^* = \frac{m}{2\pi j}}[f(z)], \tag{40}$$

$$= \lim_{z \to z^*} \frac{1}{(nm-1)!} \left(\frac{d}{dz} \right)^{nm-1} (z - z^*)^{nm} f(z). \tag{41}$$

The function $f(z)$ can be re-written in the following form

$$f(z) = \frac{g(z)}{(z - z^*)^{nm}} = \frac{(-1)^{nm} \frac{1 - \left(1 - \frac{2\pi j z}{m}\right)^{nm}}{(2\pi j)^{nm}(2\pi j z)} e^{-2\pi j z \frac{T'\sigma^2}{N_t}}}{\left(z - \frac{m}{2\pi j} \right)^{nm}}, \tag{42a}$$

$$g(z) = (-1)^{nm} \frac{1 - (1 - 2\pi j z)^{nm}}{(2\pi j)^{nm}(2\pi j z)} e^{-2\pi j z \frac{T'\sigma^2}{N_t}}. \tag{42b}$$

Then after substituting the functions in (40), we can express the integral I as

$$Q = \frac{g^{(nm-1)}(z^*)}{(nm-1)!}. \tag{43}$$

REFERENCES

[1] J. G. Andrews *et al.*, "What will 5G be?" *IEEE J. Sel. Areas Commun.*, vol. 32, no. 6, pp. 1065–1082, Jun. 2014.

[2] S. Rangan, T. S. Rappaport, and E. Erkip, "Millimeter-wave cellular wireless networks: Potentials and challenges," *Proc. IEEE*, vol. 102, no. 2, pp. 366–385, Mar. 2014.

[3] O. El Ayach, S. Rajagopal, S. Abu-Surra, Z. Pi, and R. W. Heath, "Spatially sparse precoding in millimeter wave MIMO systems," *IEEE Trans. Wireless Commun.*, vol. 13, no. 3, pp. 1499–1513, Jan. 2014.

[4] S. Akoum, O. El Ayach, and R. W. Heath, "Coverage and capacity in mmWave cellular system," in *Proc. Asilomar Conf. Signals Syst. Comput.*, Pacific Grove, CA, USA, Nov. 2012, pp. 688–692.

[5] E. Hossain, M. Rasti, H. Tabassum, and A. Abdelnasser, "Evolution toward 5G multi-tier cellular wireless networks: An interference management perspective," *IEEE Trans. Wireless Commun.*, vol. 21, no. 3, pp. 118–127, Jun. 2014.

[6] S. Singh, M. N. Kulkarni, A. Ghosh, and J. G. Andrews, "Tractable model for rate in self-backhauled millimeter wave cellular networks," *IEEE J. Sel. Areas Commun.*, vol. 33, no. 10, pp. 2196–2211, Oct. 2015.

[7] T. Bai and R. W. Heath, "Coverage in dense millimeter wave cellular networks," in *Proc. Asilomar Conf. Signals Syst. Comput.*, Pacific Grove, CA, USA, Nov. 2013, pp. 2062–2066.

[8] T. Bai and R. W. Heath, "Coverage and rate analysis for millimeter wave cellular networks," *IEEE Trans. Wireless Commun.*, vol. 14, no. 2, p. 1100–1114, Feb. 2015.

[9] G. Nigam, P. Minero, and M. Haenggi, "Coordinated multipoint in heterogeneous networks: A stochastic geometry approach," in *Proc. IEEE Global Telecommun. Conf.*, Atlanta, GA, USA, Dec. 2013, pp. 145–150.

[10] G. Nigam, P. Minero, and M. Haenggi, "Coordinated multipoint joint transmission in heterogeneous networks," *IEEE Trans. Commun.*, vol. 62, no. 11, pp. 4134–4146, Nov. 2014.

[11] J. Nam, A. Adhikary, J.-Y. Ahn, and G. Caire, "Joint spatial division and multiplexing: Opportunistic beamforming, user grouping and simplified downlink scheduling," *IEEE J. Sel. Areas Commun.*, vol. 8, no. 5, pp. 876–890, Mar. 2014.

[12] J. G. Andrews, F. Baccelli, and R. K. Ganti, "A tractable approach to coverage and rate in cellular networks," *IEEE Trans. Commun.*, vol. 59, no. 11, pp. 3122–3134, Jan. 2011.

[13] T. Bai, R. Vaze, and R. W. Heath, "Analysis of blockage effects on urban cellular networks," *IEEE Trans. Wireless Commun.*, vol. 13, no. 9, pp. 5070–5083, Sep. 2014.
[14] M. R. Akdeniz *et al.*, "Millimeter wave channel modeling and cellular capacity evaluation," *IEEE J. Sel. Areas Commun.*, vol. 32, no. 6, pp. 1164–1179, Jun. 2014.
[15] D. Tse and P. Viswanath, *Fundamentals of Wireless Communication*. Cambridge, U.K.: Cambridge Univ. Press, 2005.
[16] F. Baccelli, B. Blaszczyszyn, and P. Muhlethaler, "Stochastic analysis of spatial and opportunistic Aloha," *IEEE J. Sel. Areas Commun.*, vol. 27, no. 7, pp. 1105–1119, Sep. 2009.
[17] T. Rappaport *et al.*, "Millimeter wave communications for 5G cellular: It will work!" *IEEE Access*, vol. 1, no. 1, pp. 335–349, Aug. 2013.
[18] M. Haenggi, *Stochastic Geometry for Wireless Networks*. Cambridge, U.K.: Cambridge Univ. Press, 2013.
[19] D. Moltchanov, "Survey paper: Distance distributions in random networks," *Ad Hoc Netw.*, vol. 10, no. 6, pp. 1146–1166, Aug. 2012.
[20] L. X. Cai, X. Shen, and J. W. Mark, "REX: A randomized exclusive region based scheduling scheme for mmWave WPANs with directional antenna," *IEEE Trans. Wireless Commun.*, vol. 9, no. 1, pp. 113–121, Jan. 2010.

Diana Maamari received the Bachelor of Science and Master of Science (with high distinction) degrees in electrical engineering from the University of Balamand, Al Koura, Lebanon, and the Ph.D. degree in electrical and computer engineering from the University of Illinois at Chicago, Chicago, IL, USA, in 2009, 2011, and 2015, respectively. She has been a Senior Research and Standards Engineer with Huawei Technologies, since May 2015. Her research interests include multiuser information theory and its applications to cognitive radio channels, millimeter wave wireless networks, wireless local area networks (WLAN), and 5G networks.

Natasha Devroye received the B.Eng. degree (Hons.) in electrical engineering from McGill University, Montreal, Quebec, Canada, and the Ph.D. degree in engineering sciences from the School of Engineering and Applied Sciences, Harvard University, Cambridge, MA, USA, in 2001 and 2007, respectively. She has been an Associate Professor with the Department of Electrical and Computer Engineering, University of Illinois at Chicago (UIC), Chicago, Il, USA, since January 2009. From July 2007 to July 2008, she was a Lecturer with Harvard University. Her research interests include multiuser information theory and applications to cognitive and software-defined radio, radar, relay, and two-way communication networks. She has been an Associate Editor for the IEEE TRANSACTIONS ON WIRELESS COMMUNICATIONS, the IEEE JOURNAL OF SELECTED AREAS IN COMMUNICATIONS, and is currently an Associate Editor for the IEEE TRANSACTIONS ON COGNITIVE COMMUNICATIONS AND NETWORKING. She was the recipient of an NSF CAREER Award in 2011 and was named UIC's Researcher of the Year in the "Rising Star" category in 2012.

Daniela Tuninetti received the Ph.D. degree in electrical engineering from ENST/Telecom ParisTech, Paris, France, in 2002. She was with the Eurecom Institute, Sophia Antipolis, France. She has been an Associate Professor with the Department of Electrical and Computer Engineering, University of Illinois at Chicago (UIC), Chicago, IL, USA, since 2005. She was a Postdoctoral Research Associate with the School of Communication and Computer Science, Swiss Federal Institute of Technology in Lausanne (EPFL), Lausanne, Switzerland, from 2002 to 2004. Her research interests include ultimate performance limits of wireless interference networks, with special emphasis on cognition and user co-operation, in coexistence between radar and communication systems, in multirelay networks, and in content-type coding. She was the Editor-in-Chief of the IEEE Information Theory Society Newsletter from 2006 to 2008, the Editor for the IEEE COMMUNICATION LETTERS from 2006 to 2009, and the IEEE TRANSACTIONS ON WIRELESS COMMUNICATIONS from 2011 to 2014, and is currently an Associate Editor for the IEEE TRANSACTIONS ON INFORMATION THEORY. She was the recipient of a Best Paper Award at the European Wireless Conference in 2002, an NSF CAREER Award in 2007, and named UIC University Scholar in 2015.